applied sciences

MDPI

Communication

Heavy Metal Ion Detection Using TiO_2 Nanotubes and Self-Reduced TiO_2 Nanotube Electrodes

Cristian Pirvu [1], Mariana Prodana [1], Cristina Dumitriu [1], Alexandru-George Gheboianu [1], Andreea Madalina Pandele [1], Marius Enachescu [2,3], Gabriela-Geanina Vasile [4] and George-Octavian Buica [1,*]

[1] Department of General Chemistry, Faculty of Chemical Engineering and Biotechnologies, University Politehnica of Bucharest, 313 Splaiul Independentei, Sector 6, 060042 Bucharest, Romania; cristian.pirvu@upb.ro (C.P.); mariana.prodana@upb.ro (M.P.); cristina.dumitriu@upb.ro (C.D.); alexandru.gheboianu@stud.chimie.upb.ro (A.-G.G.); madalina.pandele@upb.ro (A.M.P.)
[2] Center for Surface Science and Nanotechnology, National University of Science and Technology Politehnica Bucharest, 313 Splaiul Independentei, Sector 6, 060042 Bucharest, Romania; marius.enachescu@cssnt-upb.ro
[3] Academy of Romanian Scientists, Splaiul Independentei 54, 050094 Bucharest, Romania
[4] National Research and Development Institute for Industrial Ecology ECOIND, 71–73 Drumul Podu Dambovitei, 060652 Bucharest, Romania; gabriela.vasile@incdecoind.ro
* Correspondence: george.buica@upb.ro

Abstract: TiO_2 nanotubes and self-reduced TiO_2 nanotube semiconductor electrodes were used for electrochemical metal ion detection in an open circuit under photo-accumulation conditions. Due to their surface properties, the electrodes showed different responses towards metal ions at different wavelengths of light radiation. Using TiO_2 nanotube-based electrodes, Pb(II) and Cu(II) ions were detected at irradiation wavelengths of 389 nm and 426 nm. Detection limits of 8×10^{-9} M and 5×10^{-9} M for Pb(II) and 3×10^{-8} and 7×10^{-9} M for Cu(II) were obtained at the two wavelengths, respectively. The self-reducing electrode showed a response to Pb(II) and Cu(II) ions when irradiated with light at 389 nm, while at 426 nm, Hg(II) ions along with Pb(II) and Cu(II) ions were detected. The obtained detection limits with self-reduced TiO_2 nanotube electrodes for Pb(II) and Cu(II) at 389 nm were 2×10^{-7} M and 8×10^{-9} M, respectively. At a wavelength of 426 nm, the detection limits were 1×10^{-7} M, 3×10^{-9}, and 4×10^{-9} M for Pb(II), Cu(II), and Hg(II), respectively.

Keywords: TiO_2 nanotube electrode; self-reduced TiO_2 nanotube electrode; heavy metal ions; photo-accumulation; electrochemical detection

Citation: Pirvu, C.; Prodana, M.; Dumitriu, C.; Gheboianu, A.-G.; Pandele, A.M.; Enachescu, M.; Vasile, G.-G.; Buica, G.-O. Heavy Metal Ion Detection Using TiO_2 Nanotubes and Self-Reduced TiO_2 Nanotube Electrodes. *Appl. Sci.* **2024**, *14*, 11879. https://doi.org/10.3390/app142411879

Academic Editors: Abdeltif Amrane, Jesús M. Anzano and María Emma Borges

Received: 16 November 2024
Revised: 15 December 2024
Accepted: 18 December 2024
Published: 19 December 2024

1. Introduction

Undoubtedly, heavy metals pose a significant risk to human health [1], so certain elements such as As, Cd, Pb, and Hg have been designated among the top 10 most dangerous substances of public health concern by the World Health Organization [2]. Due to their low clearance from the human body and significant environmental pollution from anthropogenic and human activities, the issue of detection and removal of heavy metals has become of paramount importance.

In addition to classical methods based on atomic absorption for heavy metal ion detection, electrochemical detection offers a complementary approach that excels in sensitivity, selectivity, and versatility [3]. Moreover, with the need for less complex equipment, the electrochemical approach becomes simpler to implement. Among various electrodes utilized as sensors for the detection of heavy metal ions, semiconductors have garnered significant attention due to their excellent electrochemical properties and wide range of working potentials, cost effectiveness, non-toxic nature, and, notably, their substantial geometric surface area, particularly in the form of nanostructures [4]. This unique characteristic enables them to effectively accumulate a large quantity of metal ions on their surface, leading to improved detection capabilities. From the various semiconductor materials, Ti/TiO_2 received great attention when Fujishima and Honda [5,6] unveiled its

remarkable potential in the photocatalytic splitting of water on a TiO_2 electrode under UV light irradiation. Applications for TiO_2 have emerged in a number of exciting domains in recent decades, including photovoltaics, photocatalysis, and sensors [7]. Apart from the aforementioned intrinsic benefits, nanomaterials based on TiO_2 also possess non-toxic, biocompatible, photocorrosion-resistant, and economic properties [8,9]. Furthermore, a wide range of mild temperatures and mild environmental conditions enables the production of TiO_2-based nanomaterials at a low cost, owing to the availability of a variety of nanostructures that permit an exceptionally high real surface area in relation to geometric and unique chemical, physical, and electronic properties [5,6]. Consequently, research into the structures, transmission mechanisms, and system modulation functions of TiO_2 nanomaterials for sensing applications has generated great interest [10,11].

For instance, in order to improve the sensing properties of TiO_2 nanotubes, Bessegato et al. [12] used electrochemically self-doped TiO_2 nanotubes to monitor the electrochemical oxidation of $Fe(CN)_6^{4-}$ and p-phenylenediamine, revealing them to be an excellent platform for sensors. Self-doped Ti/TiO_2 nanotube electrodes have drawn much interest as sensors because of their large surface area, improved electrical conductivity, stability, and durability. Because of its improved adsorption capacity and effective charge transfer capabilities, self-reduced TiO_2 with enhanced defect states increases the sensitivity, selectivity, and limit of detection of heavy metal ions in electrochemical sensing. Nevertheless, the applications of TiO_2 nanotubes as a sensor for the electrochemical detection of heavy metal ions are still in their infancy, and to our knowledge, only few examples based on TiO_2 oxide [13,14] or functionalized TiO_2 nanotubes [15,16] can be found in the literature. Usually, the process of electrochemical detection entails the deposition of metal ions onto the electrode surface either through controlled potential (typically employed with solid electrodes) or under open-circuit conditions (commonly used with modified electrodes). The former technique allows for the simultaneous detection of multiple ions, whereas the latter method enhances selectivity. If a semiconductor electrode is exposed to a specific wavelength in the presence of metal ions, the simultaneous processes of metal ion accumulation and reduction take place at the electrode surface, leading to an enhanced response of the electrode [17,18]. Thus, taking into account previous considerations, new insights on heavy metal ion detection using Ti/TiO_2 nanotube and self-reduced Ti/TiO_2 nanotube electrodes under photo-irradiation are being developed. The synergy between photo-accumulation and sensing using these electrodes opens up new possibilities for detecting heavy metal ions.

The integration of prior understandings is currently leading to innovative developments regarding the detection of heavy metal ions via Ti/TiO_2 nanotubes and self-reduced Ti/TiO_2 nanotube electrodes under photo-illumination. This fusion of photo-accumulation and sensing capabilities using these electrodes is paving the way for novel approaches in heavy metal ion detection.

2. Materials and Methods

The preparation of TiO_2 and reduced TiO_2 nanotube-based electrodes, as well as the accumulation of metal ions under photo-irradiation followed by their stripping, is shown in Scheme 1. Briefly, TiO_2 nanotube-based (Ti/TiO_2-NT) electrodes were obtained by electrochemical anodization at 30 V followed by thermal annealing at 450 °C for 2 h [19,20]. Subsequently, to obtain the self-reduced TiO_2 nanotube electrode (Ti/TiO_2-SR), the Ti/TiO_2-NT electrode was electrochemically reduced in 0.1 M sodium acetate (pH = 10) [21]. The accumulation and reduction of metal ions at the electrode surfaces was carried out in an open circuit under light irradiation, followed by anodic stripping and recording of the corresponding differential pulse voltammetry curves. The extended experimental section is provided in Supplementary Materials.

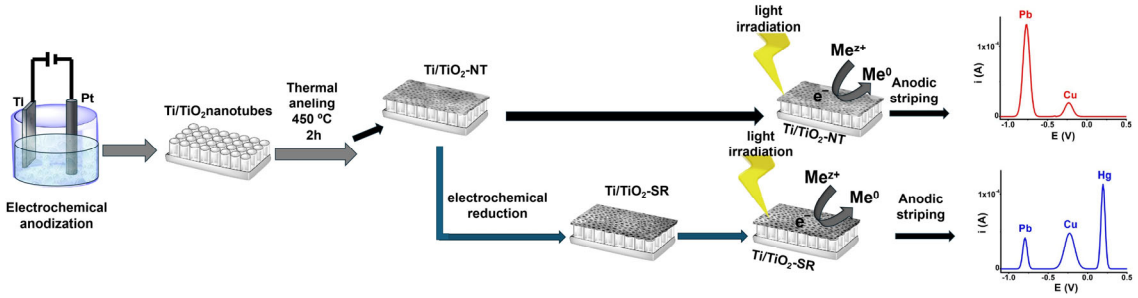

Scheme 1. Process of Ti/TiO_2-NT and Ti/TiO_2-SR electrode preparation and metal ion detection using these electrodes.

3. Results and Discussion

3.1. Electrode Characterization

The obtainment of Ti electrodes modified with TiO_2 nanotubes (Ti/TiO_2-NT) was confirmed through scanning electron microscopy analysis (Figure 1A). The surface exhibited continuous coverage with TiO_2 nanotubes, with diameters measuring 93 ± 7.5 nm and wall thicknesses of 22 ± 2.5 nm. The self-reduced TiO_2 nanotube (Ti/TiO_2-SR) electrodes showed no significant alterations in morphology post-treatment (Figure 1B). An energy dispersive X-ray analysis of the Ti/TiO_2-NT electrode showed the presence of Ti and O in a ratio of about 1:2, confirming the predominant structures of the nanotubes as that of TiO_2, while the Ti/TiO_2-NT electrode showed a decrease in oxygen content (Figure S1, see Supplementary Materials), suggesting the partial removal of oxygen atoms from the TiO_2 lattice, leading to the formation of oxygen vacancies or defects.

Furthermore, the chemical composition and oxidation state of titanium in the Ti/TiO_2-NT and Ti/TiO_2-SR electrodes were checked through X-ray photoelectron spectroscopy (XPS) analysis. Figure 1C shows the Ti2p XPS core spectra of the samples, in which two broad peaks centered at about 459.6 and 467.3 eV corresponding to the characteristic $Ti2p_{1/2}$ and $Ti2p_{3/2}$ peaks, attributed to Ti^{4+}, which is characteristic of titanium dioxide (TiO_2). As the characteristic $Ti2p_{1/2}$ and $Ti2p_{3/2}$ peaks of Ti^{3+} are located at sites slightly more negative than those of Ti^{4+}, the peaks of the Ti/TiO_2-SR exhibit a slightly negative shift in binding energy (0.2 eV) when compared to those of Ti/TiO_2-NT. This suggests the presence of a Ti^{3+} state in the lattices [22,23]. The XPS spectra of O1s showed a shoulder peak at ~532 eV, which belongs to Ti-OH species, and was observed to be slightly higher in the reduced TiO_2 nanotubes. This could indicate that oxygen vacancies are added to the TiO_2 lattice during the cathodic polarization process. The impurity level caused by Ti^{3+} self-doping is present in the TiO_2 band gap as [$O^{\bullet}$ vTi^{3+}] [24], which could enhance the photocatalytic activity in the visible range.

The UV-Vis diffuse reflectance spectra (Figure 1D) facilitated the examination of the optical absorption properties of the obtained electrodes. A subsequent conversion of the data via the Kubelka–Munk function (Figure 1D, inset) enabled the determination of their band gap. The Ti/TiO_2-NT electrode demonstrated a photo-response within the ultraviolet region (385 nm), a phenomenon attributable to the inherent band gap of TiO_2. Light scattering, pores or cracks in the nanotube arrays, or the presence of oxygen vacancies and Ti^{3+} species in the synthesized TiO_2 nanotubes may be liable for the relatively weak absorption of TiO_2 nanotubes in the visible-light spectrum. Despite modern fabrication techniques, previous research [25] has shown that the annealing process of TiO_2 nanotubes is unable to remove oxygen vacancies and Ti^{3+} species. Below the TiO_2 conduction band (CB), Ti^{3+} species can absorb visible light and hasten the formation of isolated defect energy levels. The creation of photogenerated electrons as a result of this absorption may cause a change from Ti^{3+} states to the CB of TiO_2. Upon electrochemical reduction of TiO_2 nanotubes, the introduction of Ti^{3+} centers results in additional electronic states below the conduction band. This effectively reduces the band gap from 3.31 eV to 3.21 eV, allowing TiO_2 to absorb lower-energy (longer-wavelength) photons, resulting in a bathochromic

shift (393 nm). This behavior is beneficial for improving the photocatalytic performance of the Ti/TiO_2-SR electrode by enhancing electrical conductivity (faster electron transfer) and increasing surface reactivity (better interactions between the sensor surface and heavy metal ions).

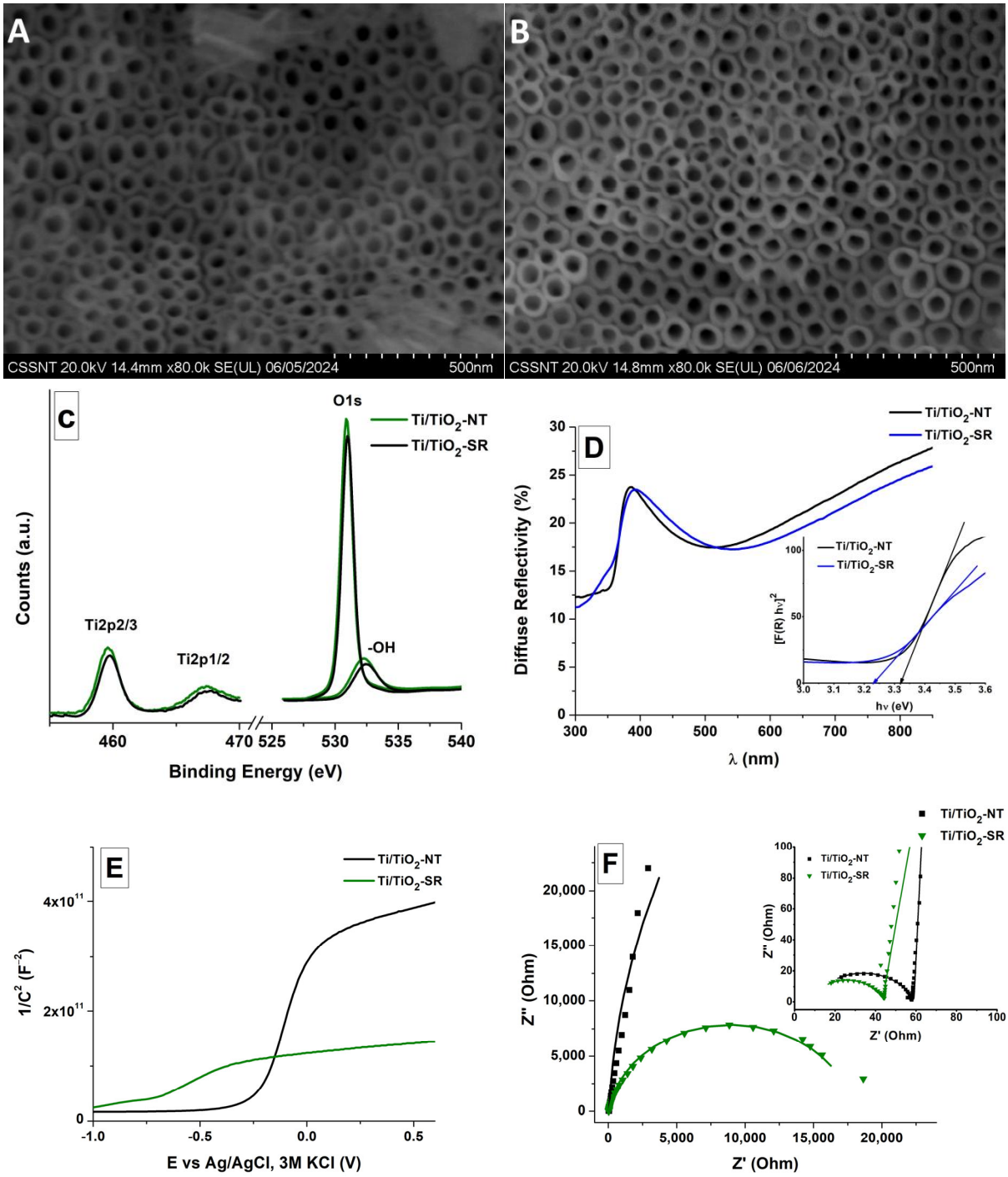

Figure 1. (**A**,**B**) Scanning electron microscopy images, (**C**) core-level XPS spectra in the Ti2p and O1s regions, (**D**) UV-Vis diffuse reflectance spectra, (**E**,**F**) Mott–Schottky and Nyquist plots of the Ti/TiO_2-NT and Ti/TiO_2-SR electrodes, respectively. Insets: (**D**) the corresponding Kubelka–Munk transformation of the diffuse reflectivity spectrum; (**F**) EIS curves in the high-frequency region.

Potential-dependent capacity measurements were performed at a frequency of 1 kHz on the Ti/TiO_2-NT and Ti/TiO_2-SR electrodes in order to clarify the impact of self-doping on the electrical characteristics of TiO_2 nanotubes. The Mott–Schottky (MS) plot is shown in Figure 1E as $1/C^2$ vs. capacity. The linear portion of the MS plot curves have positive slopes, which suggest that TiO_2 nanotube n-type semiconductor properties are unaffected by Ti^{3+} electrochemically induced self-doping. The estimated flat-band potential for Ti/TiO_2-NT is −0.27 V, and the carrier density is 4.87×10^{19} cm^{-3}. After the self-reducing process, the Ti/TiO_2-SR electrode showed a decrease in the flat-band potential (E_{fb} = −0.89 V) and an increase in the carrier density (1.61×10^{20} cm^{-3}), being in agreement with previous results [12]. Band bending is either negligible or nonexistent at the E_{fb} or the point in the semiconductor where there is no net electric field. An electron accumulation area is produced when the conduction and valence bands are bent downward at the surface, as indicated by a negative value of E_{fb}. This suggests that the semiconductor's surface may have an overabundance of electrons. The surface of reduced TiO_2 becomes less positively charged as Efb drops or may be negatively charged if the reduction is substantial. It is anticipated that the surface will have an excess of negative charge because of the buildup of electrons because our sample was reduced at a potential of −1.5 V. The positively charged metallic ions from the solution may therefore be more attracted to the negatively charged or electron-rich TiO_2 surface when the E_{fb} is lower. This would facilitate the reduction or deposition of metallic ions on the surface.

TiO_2 produces electron–hole pairs when exposed to radiation, and in reduced TiO_2, there are frequently more electrons available for reduction processes. These electrons' enhanced ability to interact with metal ions in solution is made possible by their decreased flat-band potential, which also promotes the reduction of ions and raises the possibility that they will deposit onto the TiO_2 surface. Also, the smaller band gap and lower E_{fb} increase the amount of electrons in the conduction band and lower the barrier to electron migration to the surface, hence increasing the electron transfer efficiency.

Electrochemical impedance spectroscopy measurements were performed in order to gain a better understanding of the electrodes' interfacial electrochemical behavior. Nyquist plots for the Ti/TiO_2-NT and Ti/TiO_2-SR electrodes are shown in Figure 1F. The diameter of the semicircle, which corresponds to the charge transfer resistance, is indicative of the charge transfer process at high frequencies. In comparison to the Ti/TiO_2-NT electrode, the Ti/TiO_2-SR electrode exhibits a smaller semicircle. Additionally, the resistance to electron transfer is lower in the Ti/TiO_2-SR sample when impedance data are fitted to the equivalent circuit model depicted in Figure S2 (see Supplementary Materials). The observation could potentially be attributed to the addition of Ti^{3+} doping, which enhanced the electron transfer rate between the Ti/TiO_2-SR and electrolyte interface, resulting in higher photoelectrochemical activity compared to the Ti/TiO_2-NT electrode [20].

3.2. Metal Ion Detection

To check the chemical reversibility and intermediate species formation at the Ti/TiO_2-NT and Ti/TiO_2-SR electrodes, cyclic voltammetry curves were recorded in the presence of Zn(II), Cd(II), Pb(II), Cu(II), and Hg(II) mixed ionic solution (Figure 2). At the electrode's surface, only four reduction peaks could be observed, which correspond to the reduction of Cd(II), Pb(II), Cu(II), and Hg(II) ions, respectively, to metal zero valent. In the reverse scan, the corresponding oxidation peaks are observed. The peaks are well separated in terms of potential without evidence of intermetallic species formation, probably due to the large surface of the electrode, which allows for multiple reduction sites for the ions. The absence of Zn (II) ions could be due to the start of an HER reaction at the electrode surface at lower potential.

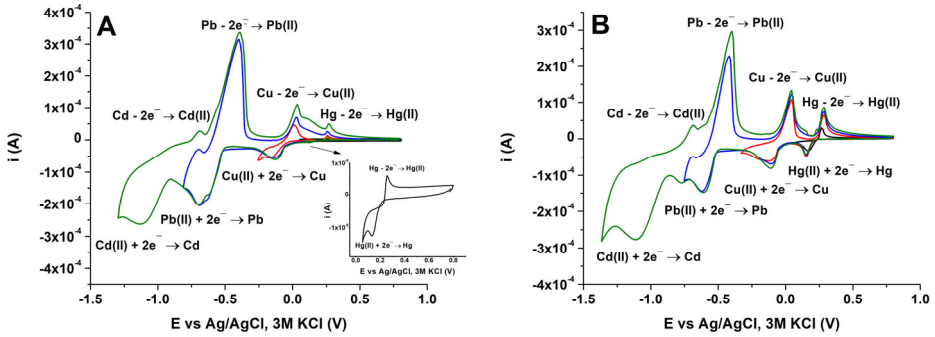

Figure 2. Cyclic voltammograms at (**A**) Ti/TiO_2-NT and (**B**) Ti/TiO_2-SR electrodes recorded in the presence of 5×10^{-4} M Zn(II), Cd(II), Pb(II), Cu(II), and Hg(II) ions at 25 mV s^{-1}.

The potential of metal ions can be tailored to the energy levels of a semiconductor's conduction band to improve the selectivity and sensitivity of electrode materials. As shown in Figure 3A, the potentials of Zn(II), Cd(II), Pb(II), Cu(II), and Hg(II) ions exceed that of the conduction band, facilitating spontaneous photoreduction under light irradiation. Both the electrode material (Ti/TiO_2-NT and Ti/TiO_2-SR) and the wavelength of light irradiation play a crucial role in the adsorption and reduction of metal ions. In the absence of UV light, due to limited adsorption as a result of oxygen's interaction with the metal ions, both electrodes showed only two minor stripping peaks at −0.76 V and −0.23 V, corresponding to Pb and Cu, respectively (Figure 3B). Conversely, exposing the electrodes to different wavelengths of light led to an increased response of the electrodes to metal ions. Furthermore, it was observed that the wavelength of light irradiation has an important influence on electrode selectivity and sensitivity. For the Ti/TiO_2-NT electrode, the stripping peak currents for Pb and Cu were found to increase upon irradiation and reach a maximum at 426 nm. The Ti/TiO_2-SR electrode showed different behavior when irradiated with different wavelengths. At 372 nm and 389 nm, the electrode responds only to Pb and Cu ions, whereas the use of irradiation at higher wavelengths (426 nm and 450 nm) led to the appearance of a new oxidation peak at around 0.2 V, which corresponds to the re-dissolution of reduced mercury (Figure 3C). This finding underlines the beneficial effect of light irradiation on the electrode surface. However, no stripping peaks were observed for Zn(II) and Cd(II) ions. Despite its theoretical feasibility, the thermodynamic driving force for the photoreduction of these ions is low. Competitive adsorption at the binding sites is probably the cause of the absence of Zn and Cd ions. This suggests that the presence of Pb(II), Cu(II), or Hg(II) ions has a significant influence on the sorption of Zn and Cd ions.

With the aim of improving the detection of metal ions on Ti/TiO_2-NT and Ti/TiO_2-SR electrodes, the influence of pH and accumulation was investigated. Figure 4A,B show the response of the Ti/TiO_2-NT and Ti/TiO_2-SR electrodes at different pH values of the metal ion photo-accumulation solution. A strong influence of pH on the electrodes' response to metal ions is observed, with the optimal response being at pH = 6. This value is in the range of the zero-charge point (PZC) of TiO_2 [26]. According to M. Zeng [26], a surface below this value is positively charged due to the presence of Ti-OH^{2+} and negatively charged (TiO^-) at pH values above 6. Therefore, below a PZC of 6, a lower response of the electrodes is observed, probably due to the electrostatic repulsions between the metal ions and the electrode surface. On the other hand, more hydroxyl groups deprotonate, and an electrostatic interaction occurs between the metal cations and hydroxyl groups at values above PZC, which has a positive effect on the complexation of metal ions by TiO_2.

Increasing the light exposure time results in increased stripping currents, as shown in Figure 4C,D. Consequently, the sensitivity of the electrodes is increased due to a larger accumulation of photoelectrons, which facilitates the deposition of a larger amount of reduced ions onto the electrode surfaces.

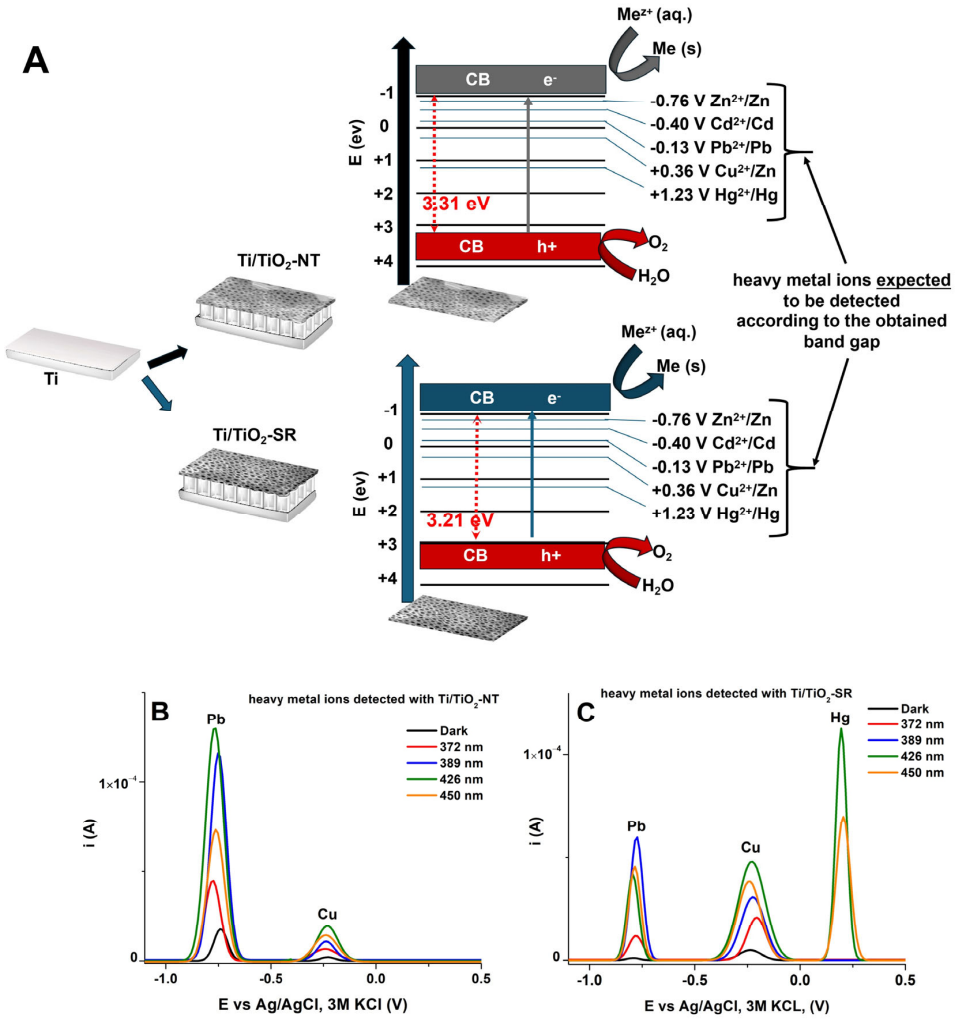

Figure 3. (**A**) A schematic of the reaction mechanism during light irradiation; DPV curves recorded on (**B**) Ti/TiO_2-NT and (**C**) Ti/TiO_2-SR electrodes at different wavelengths of irradiation light. The photo-accumulation of metal ions was performed in 4 × 10^{-6} M Zn(II), Cd(II), Pb(II), Cu(II), and Hg(II) for 30 min.

The response of the Ti/TiO_2-NT and Ti/TiO_2-SR electrodes irradiated with light at wavelengths of 389 nm and 426 nm for the simultaneous detection of Pb(II), Cu(II), and Hg (II) ions at different concentrations was evaluated under optimized conditions (Figure 5A–D). The peak currents increase with the concentration of metal ions, and their linear dependence on the concentration is shown in Figures S3 and S4 (see Supplementary Materials). The linear dependence equation of the calibration curve, the linear range, and the detection limit based on a signal-to-noise ratio of 3 are shown in Table 1 for both electrodes. The calibration curves were plotted using the mean value of triplicate results for each standard solution. The standard deviation of the results was situated in the range of 3% to 5%. As expected, the Ti/TiO_2-NT electrode only showed a response to the Pb and Cu ions at the two wavelengths used, while the Ti/TiO_2-SR electrode only showed a response to all the metal ions considered when irradiated with light of a wavelength of 426 nm. However, irradiating the electrodes with light at 426 nm results in the best response for both electrodes. The obtained electrodes demonstrated better performance when compared to earlier findings which used photo-assisted accumulation of metal ions (Table 2).

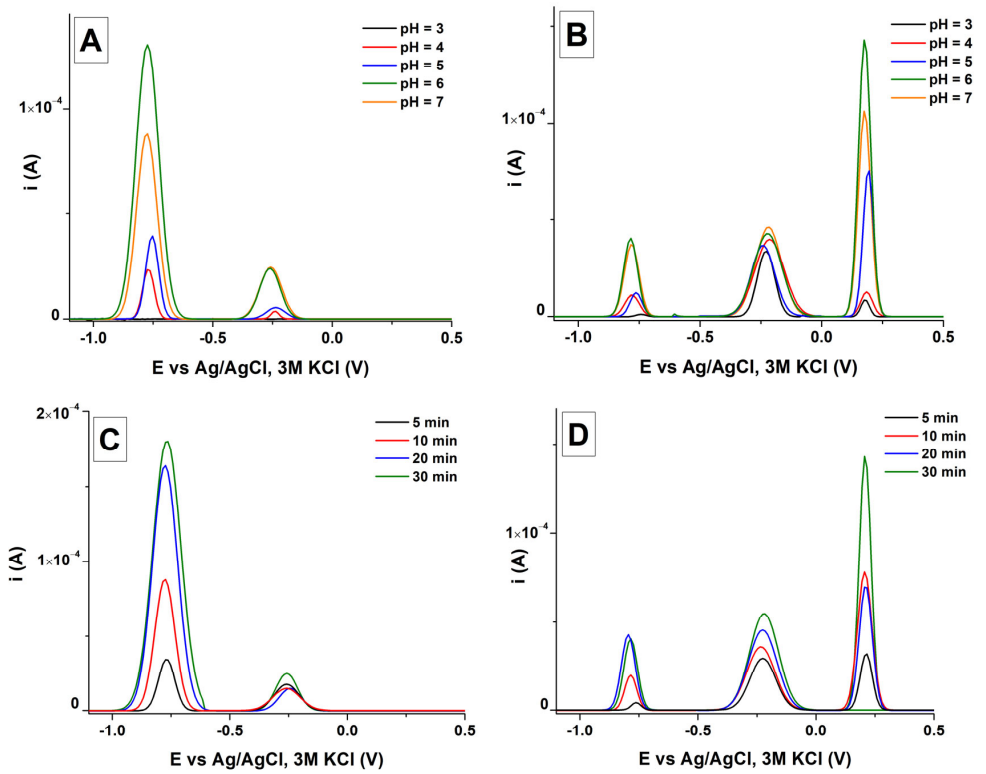

Figure 4. DPV curves recorded at (**A**,**C**) Ti/TiO_2-NT and (**B**,**D**) Ti/TiO_2-SR electrodes at different (**A**,**B**) pH values of accumulation solution and (**C**,**D**) irradiation time.

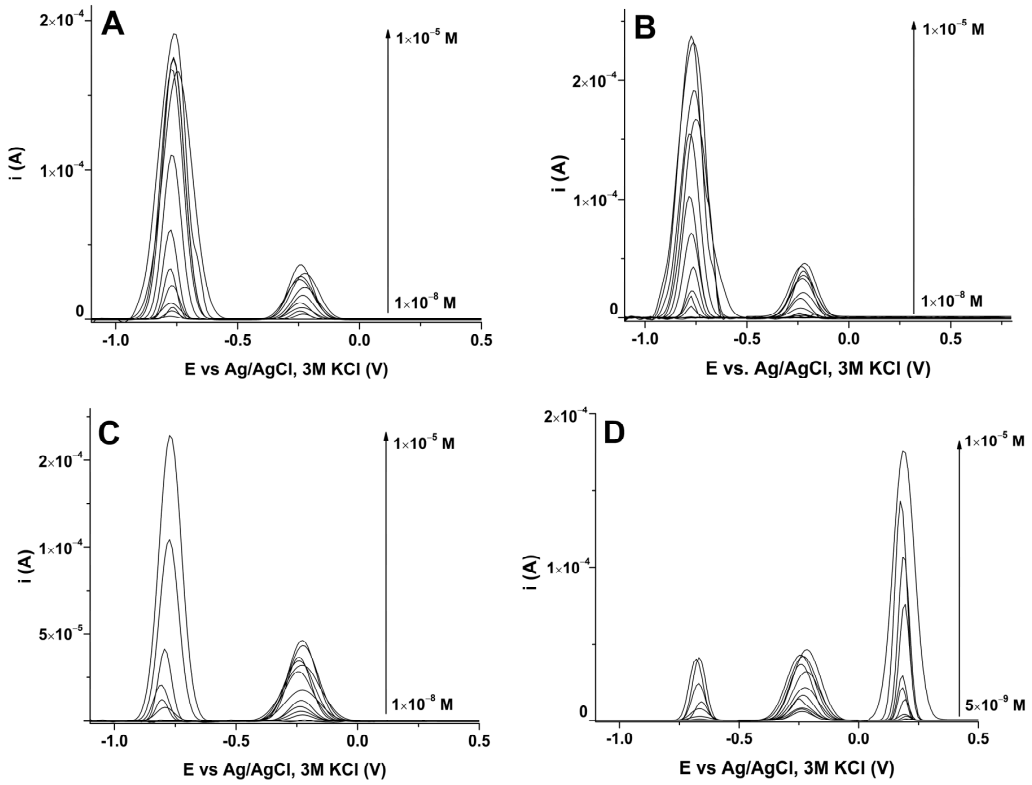

Figure 5. DPV curves at Ti/TiO_2-NT (**A**,**B**) and Ti/TiO_2-SR (**C**,**D**) electrodes for different concentrations of Pb(II), Cu(II), and Hg(II) ions under irradiation with light at wavelengths of 389 nm (**A**,**B**) and 426 nm (**C**,**D**).

Table 1. The linear dependence equation of the calibration curve, linear range, and detection limit obtained for the Ti/TiO_2-NT and Ti/TiO_2-SR electrodes at light irradiation wavelengths of 389 nm and 426 nm.

Electrode		Ti/TiO_2-NT	
Wavelength (nm)		389	
Metal Ion	Linear Dependence Equation	Linear Domain (M)	Limit of Detection (M)
Pb	$i(\mu A) = 1.82 + 1.1 \times 10^8$ C(M); $R^2 = 0.994$	$10^{-8} \div 10^{-6}$	8×10^{-9}
Cu	$i(\mu A) = 4.2 + 1.89 \times 10^7$ C(M); $R^2 = 0.990$	$5 \times 10^{-8} \div 10^{-6}$	3×10^{-8}
Wavelength (nm)		426	
Metal ion	Linear dependence equation	Linear domain (M)	Limit of detection (M)
Pb	$i(\mu A) = 15.9 + 1.42 \times 10^8$ C(M); $R^2 = 0.992$	$10^{-8} \div 10^{-6}$	5×10^{-9}
Cu	$i(\mu A) = 2.40 + 3.49 \times 10^7$ C(M); $R^2 = 0.990$	$10^{-8} \div 10^{-6}$	7×10^{-9}
Electrode		Ti/TiO_2-SR	
Wavelength (nm)		389	
Metal ion	Linear dependence equation	Linear domain (M)	Limit of detection (M)
Pb	$i(\mu A) = 1.06 + 2.1 \times 10^7$ C(M); $R^2 = 0.990$	$3 \times 10^{-7} \div 2 \times 10^{-6}$	2×10^{-7}
Cu	$i(\mu A) = 2.4 + 5.13 \times 10^7$ C(M); $R^2 = 0.994$	$5 \times 10^{-8} \div 10^{-6}$	8×10^{-9}
Wavelength (nm)		426	
Metal ion	Linear dependence equation	Linear domain (M)	Limit of detection (M)
Pb	$i(\mu A) = 0.87 + 10^7$ C(M); $R^2 = 0.989$	$2 \times 10^{-7} \div 4 \times 10^{-6}$	1×10^{-7}
Cu	$i(\mu A) = 6.5 + 5 \times 10^7$ C(M); $R^2 = 0.990$	$5 \times 10^{-9} \div 5 \times 10^{-7}$	3×10^{-9}
Hg	$i(\mu A) = 1.5 + 5.6 \times 10_7$ C(M); $R^2 = 0.992$	$5 \times 10^{-9} \div 2 \times 10^{-6}$	4×10^{-9}

Table 2. Comparison of photo-assisted heavy metal detection between the developed Ti/TiO_2-NT/ and Ti/TiO_2-SR electrodes and other previously reported electrodes.

Electrode	**Target Analyte**	**Linear Range**	**LOD**	**Ref.**
TiON/TiO_2	Pb^{2+}	10^{-5} to 10^{-1} M	10^{-5} M	[27]
$CoFe_2O_4$/CNS heterojunction-modified nickel foam	Pb^{2+} Cd^{2+}	1–10 µM 1–10 µM	0.213 µM 0.316 µM	[28]
Glassy carbon/poly(2,2′-(ethan-1,2-diylbis((2-(azulen-2-ylamino)-2-oxoethyl)azandiyl))diacetic acid	Cu^{2+} Hg^{2+}	0.003–2µM 0.005–1µM	0.4 nM 0.7 nM	[18]
Metal-free g-C3N4/carbon black composite	Cd^{2+} Pb^{2+} Hg^{2+}	0–0.7 µM 0–0.3 µM 0–0.5 µM	2.1 nM 0.26 nM 0.22 nM	[29]
Zr/ZrO_2 nanotube	Pb^{2+} Cu^{2+} Hg^{2+}	0.08–10 µM 0.05–2 µM 0.4–10 µM	50 nM 40 nM 100 nM	[17]
Ti/TiO_2	Cd^{2+} Pb^{2+} Cu^{2+}	0.6–13.2 µM 0.6–13.2 µM 0.6–13.2 µM	160 nM 140 nM 100 nM	[13]
Ti/TiO_2 nanotubes	Pb^{2+} Cu^{2+}	0.01–1 µM 0.01–1 µM	5 nM 7 nM	This work
Ti/TiO_2 self-reduced nanotubes	Pb^{2+} Cu^{2+} Hg^{2+}	0.2–4 µM 0.005–0.5 µM 0.005–2 µM	100 nM 3 nM 4 nM	This work

4. Conclusions

Ti/TiO_2 nanotubes and self-reduced TiO_2 nanotube electrodes were used to create a novel photo-accumulation and sensing system for detecting trace amounts of heavy metals. The obtained results show that metal ions can be simultaneously detected in an aqueous solution through photoreduction-induced metal ion deposition on Ti/TiO_2 nanotube electrodes under light irradiation. In addition, the wavelength of the irradiation light plays a very important role in the selectivity of the electrode due to its surface properties. Nevertheless, the structure of TiO_2 nanotubes offers further opportunities for improvement to achieve higher selectivity by tuning their surface and reducing the band gap of the material, which could enable the use of irradiation light in the visible wavelength range.

Supplementary Materials: The following supporting information can be downloaded at https://www.mdpi.com/article/10.3390/app142411879/s1, Figure S1: Energy dispersive X-ray spectra for (A) Ti/TiO_2-NT and (B) Ti/TiO_2-SR electrodes; Figure S2: The equivalent circuit model used for fitting the EIS experimental data for the Ti/TiO_2-NT and Ti/TiO_2-SR electrodes; Figure S3: The calibration curves obtained from the Ti/TiO_2-NT electrodes for different concentrations of (A,C) Pb(II) and (B,D) Cu(II) ions. The accumulation of metal ions was performed under light irradiation at 389 nm (A,B) and 426 nm (C,D). Insets: the corresponding linear domain of concentration; Figure S4: The calibration curves obtained from the Ti/TiO_2-NT electrodes for different concentrations of (A,C) Pb(II), (B,D) Cu(II), and (E) Hg(II) ions. The accumulation of metal ions was performed under light irradiation at 389 nm (A,B) and 426 nm (C–E). Insets: the corresponding linear domain of concentration.

Author Contributions: Conceptualization, C.P and G.-O.B.; methodology, G.-O.B.; software, C.D. and A.M.P.; validation, G.-O.B. and G.-G.V.; formal analysis, A.-G.G., M.P. and C.D.; investigation, A.M.P., A.-G.G., M.P. and M.E.; data curation, C.P., M.E. and G.-O.B.; writing—original draft preparation, C.P. and G.-O.B.; writing—review and editing, C.P., M.E. and G.-O.B.; visualization, G.-O.B. and C.D.; supervision, G.-O.B.; project administration, G.-O.B. All authors have read and agreed to the published version of the manuscript.

Funding: This research received no external funding.

Institutional Review Board Statement: Not applicable.

Informed Consent Statement: Not applicable.

Data Availability Statement: The original contributions presented in this study are included in this article; further inquiries can be directed to the corresponding author.

Acknowledgments: This work was supported by a grant from the National Program for Research of the National Association of Technical Universities—GNAC ARUT 2023.

Conflicts of Interest: The authors declare no conflicts of interest.

References

1. Budi, H.S.; Catalan Opulencia, M.J.; Afra, A.; Abdelbasset, W.K.; Abdullaev, D.; Majdi, A.; Taherian, M.; Ekrami, H.A.; Mohammadi, M.J. Source, toxicity and carcinogenic health risk assessment of heavy metals. *Rev. Environ. Health* **2024**, *39*, 77–90. [CrossRef] [PubMed]
2. World Health Organization. International Programme on Chemical Safety, Health Impacts of Chemicals. 2020. Available online: https://www.who.int/news-room/photo-story/photo-story-detail/10-chemicals-of-public-health-concern (accessed on 15 October 2024).
3. Gezahegn, T.F.; Ambaye, A.D.; Mekoyete, T.M.; Malefane, M.E.; Oyedotun, K.O.; Mokrani, T. Breakthroughs in nanostructured-based chemical sensors for the detection of toxic metals. *Talanta Open* **2024**, *10*, 100354. [CrossRef]
4. Nigam, A.; Sharma, N.; Tripathy, S.; Kumar, M. Development of semiconductor based heavy metal ion sensors for water analysis: A review. *Sens. Actuators A Phys.* **2021**, *330*, 112879. [CrossRef]
5. Fujishima, A.; Honda, K. Electrochemical photolysis of water at a semiconductor electrode. *Nature* **1972**, *238*, 37–38. [CrossRef]
6. Fujishima, A.; Rao, T.N.; Tryk, D.A. Titanium dioxide photocatalysis. *J. Photochem. Photobiol. C Photochem. Rev.* **2000**, *1*, 1–21. [CrossRef]

7. Zakir, O.; Ait-Karra, A.; Idouhli, R.; Khadiri, M.; Dikici, B.; Aityoub, A.; Abouelfida, A.; Outzourhit, A. A review on TiO_2 nanotubes: Synthesis strategies, modifications, and applications. *J Solid State Electrochem.* **2023**, *27*, 2289–2307. [CrossRef]
8. Ikreedeegh, R.R.; Hossen, M.A.; Tahir, M.; Aziz, A.A. A comprehensive review on anodic TiO_2 nanotube arrays (TNTAs) and their composite photocatalysts for environmental and energy applications: Fundamentals, recent advances and applications. *Coord. Chem. Rev.* **2024**, *499*, 215495. [CrossRef]
9. Thennarasu, G.; Rajendran, S.; Kalairaj, A.; Rathore, H.S.; Panda, R.C.; Senthilvelan, T. A comprehensive review on the application of semiconductor nanometal oxides photocatalyst for the treatment of wastewater. *Clean Technol. Environ. Policy.* **2024**, 1–22. [CrossRef]
10. Qiu, J.; Zhang, S.; Zhao, H. Recent applications of TiO_2 nanomaterials in chemical sensing in aqueous media. *Sens. Actuators B Chem.* **2021**, *160*, 875–890. [CrossRef]
11. Zhao, J.; Wang, H.; Cai, Y.; Zhao, J.; Gao, Z.; Song, Y.-Y. The challenges and opportunities for TiO_2 nanostructures in gas sensing. *ACS Sens.* **2024**, *9*, 1644–1655. [CrossRef]
12. Bessegato, G.G.; Hudari, F.F.; Zanoni, M.V.B. Self-doped TiO_2 nanotube electrodes: A powerful tool as a sensor platform for electroanalytical applications. *Electrochim. Acta* **2017**, *235*, 527–533. [CrossRef]
13. Ma, H.; An, R.; Chen, L.; Fu, Y.; Ma, C.; Dong, X.; Zhang, X. A study of the photodeposition over Ti/TiO_2 electrode for electrochemical detection of heavy metal ions. *Electrochem. Commun.* **2015**, *57*, 18–21. [CrossRef]
14. Suárez, M.F.; Mills, A.; Egdell, R.G.; Compton, R.G. Anodic stripping voltammetry with photochemical preconcentration at nanocrystalline TiO_2 films: Detection of Ag^+ and Hg^{2+}. *Electroanalysis* **2000**, *12*, 413–419. [CrossRef]
15. Liu, M.; Zhao, G.; Tang, Y.; Yu, Z.; Lei, Y.; Li, M.; Zhang, Y.; Li, D. A simple, stable and picomole level lead sensor fabricated on DNA-based carbon hybridized TiO_2 nanotube arrays. *Environ. Sci. Technol.* **2010**, *44*, 4241–4246. [CrossRef]
16. Yang, L.; Luo, S.; Su, F.; Xiao, Y.; Chen, Y.; Cai, Q. Carbon-nanotube-guiding oriented growth of gold shrubs on TiO_2 nanotube arrays. *J. Phys. Chem. C* **2010**, *114*, 7694–7699. [CrossRef]
17. Buica, G.-O.; Stoian, A.B.; Manole, C.; Demetrescu, I.; Pirvu, C. Zr/ZrO_2 nanotube electrode for detection of heavy metal ions. *Electrochem. Commun.* **2020**, *110*, 106614. [CrossRef]
18. Pirvu, C.; Stanciu, G.; Buica, G.-O. Cu(ii) and Hg(ii) detection under photo-assisted accumulation in an open circuit potential at a polyazulene–EDTA like modified electrode. *Analyst* **2022**, *147*, 4730–4734. [CrossRef] [PubMed]
19. Dumitriu, C.; Pirvu, C.; Demetrescu, I. The Electrochemical Formation and Shielding Mechanism of TiO_2 Nanotubes in Organic Electrolytes with Different Viscosity. *J. Electrochem. Soc.* **2013**, *160*, G55. [CrossRef]
20. Manovah David, T.; Ranjan Dev, P.; Wilson, P.; Sagayaraj, P.; Mathews, T. A critical review on the variations in anodization parameters toward microstructural formation of TiO_2 nanotubes. *Electrochem. Sci. Adv.* **2022**, *2*, e202100083. [CrossRef]
21. Spanu, D.; Dhahri, A.; Binda, G.; Monticelli, D.; Pinna, M.; Recchia, S. Ultrafast electrochemical self-doping of anodic titanium dioxide nanotubes for enhanced electroanalytical and photocatalytic performance. *Chemosensors* **2023**, *11*, 560. [CrossRef]
22. Xing, M.; Fang, W.; Nasir, M.; Ma, Y.; Zhang, J.; Anpo, M. Self-doped Ti^{3+}-enhanced TiO_2 nanoparticles with a high-performance photocatalysis. *J. Catal.* **2013**, *297*, 236–243. [CrossRef]
23. Liao, W.; Yang, J.; Zhou, H.; Murugananthan, M.; Zhang, Y. Electrochemically self-doped TiO_2 nanotube arrays for efficient visible light photoelectrocatalytic degradation of contaminants. *Electrochim. Acta* **2014**, *136*, 310–317. [CrossRef]
24. Xing, M.; Zhang, J.; Chen, F.; Tian, B. An economic method to prepare vacuum activated photocatalysts with high photo-activities and photosensitivities. *Chem. Commun.* **2011**, *47*, 4947–4949. [CrossRef] [PubMed]
25. Guo, Z.; Prezhdo, O.V.; Hou, T.; Chen, X.; Lee, S.; Li, Y. Fast energy relaxation by trap states decreases electron mobility in TiO_2 nanotubes: Time-domain Ab initio analysis. *J. Phys. Chem. Lett.* **2014**, *5*, 1642–1647. [CrossRef] [PubMed]
26. Zeng, M. Influence of TiO_2 surface properties on water pollution treatment and photocatalytic activity. *Bull. Korean Chem. Soc.* **2013**, *34*, 953–956. [CrossRef]
27. Elsayed, A.M.; Ahmed, A.M.; Tammam, M.T.; Eissa, M.F.; Aly, A.H. Sensing of heavy metal Pb^{2+} ions in water utilizing the photonic structure of highly controlled hexagonal $TiON/TiO_2$ nanotubes. *Sci. Rep.* **2024**, *14*, 1015. [CrossRef]
28. Xie, F.; Tang, F.; Li, X.; Wu, X.; Wang, S.; Xie, H.; Wang, P.; Li, Y.; Liu, Q. Photo-assisted "co-movement catalysis": $CoFe_2O_4$/CNS heterojunction based portable electrochemical sensor for simultaneous detection of Pb^{2+} and Cd^{2+} in natural water. *J. Hazard. Mater.* **2023**, *460*, 132420. [CrossRef] [PubMed]
29. Hu, J.; Li, Z.; Zhai, C.; Zeng, L.; Zhu, M. Photo-assisted simultaneous electrochemical detection of multiple heavy metal ions with a metal-free carbon black anchored graphitic carbon nitride sensor. *Anal. Chim. Acta* **2021**, *1183*, 338951. [CrossRef]